Molecular Modeling of Nearly Full-Length ErbB2 Receptor

Péter Bagossi,* Gábor Horváth,† György Vereb,† János Szöllösi,†‡ and József Tőzsér*
Departments of *Biochemistry and Molecular Biology, †Biophysics and Cell Biology, and ‡Cell Biophysical Research Group of Hungarian Academy of Sciences, Research Center for Molecular Medicine, Medical and Health Science Center, University of Debrecen, Hungary

ABSTRACT Members of the epidermal growth factor receptor family play important roles in various cellular processes, both in physiological and in pathological conditions. Dimerization and autophosphorylation of these receptor tyrosine kinases are key events of signal transduction. Details of the molecular events of the signaling are not entirely known. To facilitate the understanding of receptor structure and function at the molecular level, a molecular model was built for the nearly full-length ErbB2 dimer. Modeling was based on the x-ray or nuclear-magnetic resonance structures of extracellular, transmembrane, and intracellular domains. The extracellular domain was positioned above the cell membrane based on the distance determined from experimentally measured fluorescence resonance energy transfer. Favorable dimerization interactions are predicted for the extracellular, transmembrane, and protein kinase domains in the model of a nearly full-length dimer of ErbB2, which may act in a coordinated fashion in ErbB2 homodimerization, and also in heterodimers of ErbB2 with other members of the ErbB family.

INTRODUCTION

Members of the epidermal growth factor receptor (EGFR) family receptor tyrosine kinases play important roles in cell proliferation, differentiation, apoptosis, and migration. The four known members of the family: ErbB1 (EGFR), ErbB2 (HER2/Neu), ErbB3 (HER3), and ErbB4 (HER4) may act as signal transducers at the cell membrane and initiate a complex network of processes inside the cell in response to extracellular signals (Marmor et al., 2004; Schlessinger, 2000; Yarden, 2001). Dysfunctions of these proteins result in several diseases such as cancer, diabetes, immune deficiencies, and cardiovascular diseases (Blume-Jensen and Hunter, 2001). Various approaches have been developed to therapeutically target ErbB proteins, including monoclonal antibodies, synthetic tyrosine kinase inhibitors, toxin conjugates, and antisense oligonucleotides (de Bono and Rowinsky, 2002).

Unlike other ErbB receptors, ErbB2 has no known ligand (Yarden, 2001). However, its amplification can cause breast, ovarian, gastric, and salivary cancers (Koeppen et al., 2001; Press et al., 1994; Slamon et al., 1987, 1989). Overexpression of ErbB2 can occur in 25–30% of breast cancers and correlates with an aggressive tumor phenotype (Paik and Liu, 1999; Ross and Fletcher, 1998). An anti-ErbB2 antibody, Herceptin (Trastuzumab) (Carter et al., 1999, 1992; Ranson and Sliwkowski, 2002) is now in clinical use against metastatic breast cancer overexpressing ErbB2; however, 70% of patients are resistant to this treatment (Kute et al., 2004). In contrast to Herceptin, the anti-ErbB2 antibody 2C4 is promising even in those types of cancer where ErbB2 receptor surface density is not very high (Jackson et al., 2004). Other approaches to break ErbB2-mediated signaling, such as antibody-coupled cytotoxic agents, specific small-molecule tyrosine kinase inhibitors, antisense and interfering oligonucleotides, as well as gene therapy, are also actively investigated (de Bono and Rowinsky, 2002).

The ErbB receptors show close homology in their sequence and domain organization: they have an ~600-residue-long extracellular region with four domains responsible for ligand binding, a single transmembrane helix, and an ~500-residue-long intracellular region with the most conserved tyrosine kinase domain, followed by a less conserved regulatory tail at the C-terminal end of the protein. Within a given cell type, ErbB receptors are expressed at various levels and they can form homo- and heterodimers or higher order oligomers at the cell surface (Yarden, 2001). Although ErbB2 has no known ligand, it is the most preferred oligomerization partner, and its associated form with tyrosine-kinase-defective ErbB3 shows the highest signal transducing potential among the ErbB family (Citri et al., 2003). Dimerization/oligomerization plays a critical role in the activation of the kinase domain by bringing the two catalytic domains close enough for transphosphorylation of the kinase domain itself, and further tyrosine residues on the C-terminal regulatory domain (Vereb et al., 2002). Recently, several structural studies on ErbB1–4 domains were published in responses to the great demand to understand the biology of ErbB receptors: crystal structures of extracellular domains of ErbB1 (Ferguson et al., 2003; Garrett et al., 2002; Ogiso et al., 2002), ErbB2 (Cho et al., 2003; Garrett et al., 2003), and ErbB3 (Cho and Leahy, 2002), and the intracellular protein kinase domain of ErbB1 (Stamos et al., 2002) have been determined, together with the NMR structure of the transmembrane helix of ErbB2 (Goetz et al., 2001).

Submitted May 14, 2004, and accepted for publication November 22, 2004.

Péter Bagossi and Gábor Horváth contributed equally to this work.

Address reprint requests to Péter Bagossi, the Department of Biochemistry and Molecular Biology, Research Center for Molecular Medicine, Medical and Health Science Center, University of Debrecen, H-4012 Debrecen, POB 6, Hungary. Tel.: 36-52-416-432; Fax: 36-52-314-989; E-mail: peter@indi.biochem.dote.hu.

0006-3495/05/02/1354/10 $2.00

doi: 10.1529/biophysj.104.046003

Fluorescence resonance energy transfer (FRET) measurements are very suitable for studying conformation and associations of biomolecules (Szöllösi et al., 2002, 1984; Trón et al., 1984). FRET measurements between fluorescently labeled monoclonal antibodies on the living cells provide useful information about proximity relationships of cell surface proteins. The rate of the FRET process depends on the inverse sixth power of the actual separation distance of donor and acceptor dyes and on their mutual orientation factor (Förster, 1948, 1949; Szöllösi et al., 2002). A method for constructing two-dimensional maps of receptor distributions on the basis of FRET data was described, and maps were constructed for major histocompatibility complex class I and II, interleukin-2 receptor, transferrin receptor, intercellular adhesion molecule-1, and ErbB receptors (Szöllösi et al., 2002; Vereb et al., 2003).

Combinations of FRET data and molecular modeling can provide hints about the possible orientation and arrangements of membrane proteins. Previously, we have successfully used the same methodology to predict dimeric and tetrameric arrangements in a supramolecular cluster of the major histocompatibility complex class I, CD8, and T-cell receptor localized between an antigen-presenting cell and a T-cell (Gáspár et al., 2001). In the present report we have assembled the domains of ErbB2 with known structures to construct a model for the nearly full-length molecule with the help of molecular modeling methods, and have positioned the assembled ErbB2 in the lipid bilayer of the cell membrane based on FRET measurements.

MATERIALS AND METHODS

Cell lines

The human gastric cancer cell line N87 and human breast cancer cell line SK-BR-3 were obtained from the American Type Culture Collection (Rockville, MD) and grown according to their specification to confluency. For flow cytometry, cells were harvested by trypsin-EDTA treatment.

Fluorescent conjugation of Herceptin Fab′

The Herceptin Fab′ fragment was a kind gift of Genentech (South San Francisco, CA). The Herceptin Fab′ was a mutated version containing an SH-group opposite to the binding site which was conjugated with an SH-reactive dye at 1:1 molar ratio for exact calculation of FRET distances. Aliquots of Herceptin Fab′ (at least at 1 mg/ml concentration) were conjugated with a maleimide derivative of fluorescein (Alexa-488; Molecular Probes, Eugene, OR) and of sulfoindocyanine (Cy3 and Cy5) (Amersham, Brauschweig, Germany), as described previously (Szöllösi et al., 1996).

Labeling of cells with fluorescent Fab′s

Freshly harvested cells were washed twice in ice-cold phosphate-buffered saline (PBS), pH 7.4. The cell pellet was suspended in 25 μl of PBS (final concentration 10^6 cells/sample) and incubated with 25 μl of Alexa-488-conjugated Fab′ for 30 min on ice. The excess of Fab′ was at least fivefold above the K_d during the incubation (i.e., at saturating concentrations). The same procedure was used for the determination of intermolecular distances between ErbB2 molecules with Cy3- and Cy5-labeled Herceptin Fab′, adding the same concentration of both antibodies simultaneously to the cell pellet. Special care was taken to keep the cells on ice before FRET analysis to avoid significant protein internalization. The labeled cells were washed twice with excess of cold PBS.

Labeling of cells with lipid probes

The surface of cells was labeled for FRET-based vertical distance measurements with 2-(4,4-difluoro-5-(4-phenyl-1,3-butadienyl)-4-bora-3a,4a-diaza-*s*-indacene-3-pentanoyl)-1-hexadecanoyl-*sn*-glycero-3-phosphatidylcholine (BODIPY-PC, 581/591; Molecular Probes, Eugene, OR) as acceptor for Alexa-488-conjugated Fab′ bound to the ErbB2 receptor. For labeling with BODIPY-PC (581/591), a final concentration of up to 5 μg/ml of dye was added to the cell suspension kept in glass tubes, at a cell density of 10^6 cells/sample (in 50 μl final volume). Labeling was performed for 30 min on ice, then cells were washed twice with ice-cold PBS, labeled with Fab′ for 30 min on ice, and analyzed immediately by flow cytometry. Cells were kept in ice-cold buffer (without fixation) during the flow cytometric analysis.

Flow cytometric resonance energy transfer measurements

The FRET efficiency was determined using flow cytometry by measuring the extent of both donor-quenching and acceptor sensitization through detecting spectrally selected fluorescence intensities on a cell-by-cell basis, as described in details earlier (Sebestyén et al., 2002; Szöllösi et al., 1984; Trón et al., 1984). To determine the homoassociation of ErbB2 molecules, four samples were run: 1), unlabeled cells; 2), donor-only labeled cells; 3), acceptor-only labeled cells; and 4), donor- and acceptor-labeled cells. Single stained samples served as controls for determining the spectral overspill of donor and acceptor dyes, as well as nonspecific cross-excitation of the dyes that can occur with two-laser illumination. Measurements were carried out on a FACSCalibur flow cytometer (BD Biosciences, San Jose, CA), where dual laser excitation at 488 and 635 nm was applied to determine energy transfer efficiency. Three fluorescence parameters were detected simultaneously from each experimental sample: 1), specific donor dye fluorescence in FL2 (585/42 BP) upon 488 nm excitation (Cy3), 2), the fluorescence signal excited at 488 nm and detected in FL3 (670 LP), which in addition to the sensitized emission of the acceptor contains spectral overlap from the donor and from the directly excited acceptor, and 3), direct acceptor dye emission (Cy5) in FL4 (661/16 BP) upon 635 nm excitation. The transfer efficiency values (E) were determined on a cell-by-cell basis using the AFlex software (Szentesi et al., 2004) and presented as approximately normally distributed, unimodal energy transfer efficiency histograms of 20,000 cells (Fig. 1). The mean values of energy transfer efficiency histograms of three independent sets of samples were used for distance determination. Intermolecular distances (R) were calculated using Förster's inverse sixth-power distance-dependence law of energy transfer efficiency (E) as follows: $R = R_0(1/E\text{-}1)^{1/6}$, with a value of 5.0 nm for the R_0 Förster critical distance of the Cy3–Cy5 donor-acceptor pair (Bastiaens and Jovin, 1996).

In the case of protein/lipid FRET measurements, the fluorescent proteins are surrounded by a large array of acceptor-labeled lipids; therefore, the efficiency of FRET is also a function of the donor/acceptor ratio. In such a situation, only the perpendicular distance of labeled epitope from the cell membrane surface is estimated according to the theory and model described by Yguerabide (1994). The membrane proximity experiments were carried out on a FACStar^{PLUS} flow cytometer (BD Biosciences) with 488 and 514 nm laser excitations. Three fluorescence parameters were detected simultaneously from each experimental sample: 1), specific donor dye fluorescence in FL1 (540/40 BP) upon 488-nm excitation (Alexa-488); 2), the fluorescence emission excited at 488 nm and detected in FL2 (590 LP); and 3), fluorescence emission excited at 514 nm and detected in FL4 (590 LP).

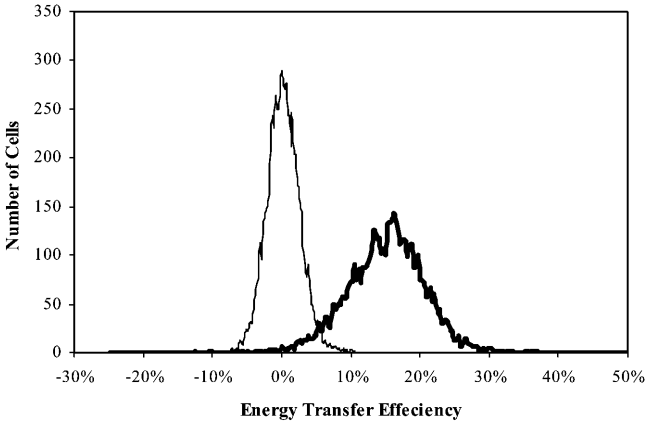

FIGURE 1 Representative energy transfer efficiency histogram of the homoassociation of Herceptin Fab′ (*bold line*) and negative control of donor-only labeled sample (*thin line*) on living N87 gastric tumor cells as measured on the FACSCalibur flow cytometer (BD Biosciences). To detect homoassociation, both donor (Cy3)- and acceptor (Cy5)-labeled Herceptin Fab's were added simultaneously to unfixed cells, whereas only Cy3-Herceptin Fab′ was added as negative control. The mean ± SD of the unimodal energy transfer efficiency distribution was used for distance calculations.

The *E*-values were determined on a cell-by-cell basis using the AFlex software (Szentesi et al., 2004). The fractional change in donor intensity, defined as $E/(1\text{-}E) = I_D/I_{DA}\text{-}1$, was plotted against the surface density of BODIPY-PC, and the experimental data were fitted with a straight line (Fig. 2). The average of the slopes from three independent experiments was used to determine the K_q quenching constant, from which the distance of closest approach, $R = R_0^{3/2}(\pi/2K_q)^{1/4}$, was computed. The validity of the model has been proved by Valenzuela et al. (1994) using the acetylcholine receptor system. A value of 5.6 nm was used for the R_0 Förster critical distance based

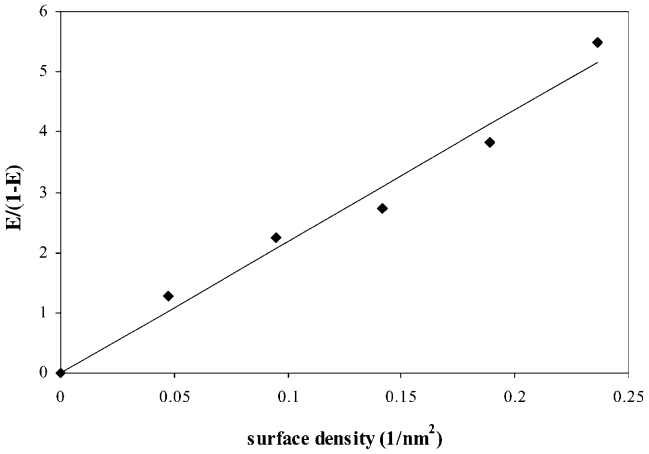

FIGURE 2 Stern-Volmer plot for the determination of the distance from the membrane of Alexa-488-labeled Herceptin Fab′ attached to ErbB2 molecules on living N87 cells. The derived $E/(1\text{-}E)$ values are plotted against the surface density of our lipid probe, BODIPY-PC (581/591) used as a FRET acceptor. The experimentally determined points, obtained from means of energy transfer efficiency histograms, were fitted with a straight line, whose slope was used to determine membrane proximity of the Herceptin Fab′ (for details, see Materials and Methods). The plot is representative of three similar measurements.

on the emission and excitation spectra of Alexa-488 and BODIPY-PC (581/591), respectively. The surface density of BODIPY-PC was calculated from the applied dye and cell concentrations assuming a total dye uptake by the outer leaflet of the cell membrane (confirmed by microscopy and fluorimetric measurement of the cells and the labeling supernatant). In our method of calculating energy transfer, a special coefficient, the so-called α-factor, has to be used that can be determined empirically from two samples labeled either with donor or with acceptor only, using the same antigen as the target, expressed at high numbers at the cell surface. This approach provides for an equal number of donor- and acceptor-bearing antibodies in the samples, as well as good signal/noise ratio, which, with the knowledge of dye/antibody ratios allows the placement of ET efficiency values onto an absolute scale. In our case, a 1:1 donor/acceptor ratio was difficult to establish, since we were using a protein and a lipid probe and no fluorophores matching the spectral characteristics of the acceptor were available. Therefore we used a standard (a Fab of W6/32, binding to the heavy chain of class I HLA A, B, C molecules) with known vertical distance from the plasma membrane (6.2 nm, Gáspár et al., 2001) to calibrate our system. A similar slope was obtained for W6/32 Fab as seen on Fig. 2 (data not shown). Using this slope and the known distance, we derived the correct calibrated α-factor, which in turn was used to calculate the energy transfer efficiencies for the Herceptin Fab′. This approach was confirmed later in an independent experiment on a more sensitive flow cytometer (FACSVantage SE with DiVa option, BD Biosciences), when α-factor was directly estimated and used for calculating transfer efficiency. The number of surface antigens (ErbB2 receptor) was determined by a Spherotec rainbow bead with eight fluorescence peaks (G. Kisker GbR, Steinfurt, Germany). The number of lipid probes was estimated from its surface density, which was determined as described above. With this new, independent calibration method, we obtained 7.7 nm for the membrane proximity of Herceptin-Fab′, which is the same (within the error limit) as we determined with the other method using W6/32 as a reference.

Construction of models for ErbB2 domains

Crystal structures of ErbB2 and ErbB1 ectodomains (PDB accession codes: 1N8Z, Cho et al., 2003; and 1IVO, Ogiso et al., 2002, respectively) were downloaded from the Protein Data Bank (Berman et al., 2000). Invisible loops were built by MODELLER (Sali and Blundell, 1993) and SYBYL (Tripos, St. Louis, MO).

NMR structure of the transmembrane helix of ErbB2 (PDB accession code: 1IIJ, Goetz et al., 2001) was used together with templates from the transmembrane regions of Glycophorin A (PDB accession code: 1AFO, MacKenzie et al., 1997), photosynthetic reaction center (PDB accession code: 1PRC, Deisenhofer et al., 1995), and bacteriorhodopsin (PDB accession code: 1AP9, Pebay-Peyroula et al., 1997) for construction of transmembrane helix dimers.

The following secondary structure prediction methods were applied for the inner juxtamembrane region, located between the transmembrane and the protein kinase domains: GOR (Garnier et al., 1978), Maxfield-Scheraga (Maxfield and Scheraga, 1976), and Qian-Sejnowski (Qian and Sejnowski, 1988) methods as implemented in SYBYL; and GOR4 (Garnier et al., 1996), SOPMA (Geourjon and Deleage, 1995), JNET (Cuff and Barton, 1999), and HNN (Guermeur et al., 1999), which were available on the ExPASy molecular biology server (http://www.expasy.org). The ExPASy server was also used for BLAST sequence similarity search.

The homologous model for the protein kinase domain of ErbB2 was built by MODELLER based on the crystal structure of the protein kinase domain of ErbB1 (Stamos et al., 2002) and the sequence alignment made by CLUSTALW (Thompson et al., 1994).

To eliminate some large unfavorable van der Waals interactions generated by modeling, short minimizations were applied at several stages of the procedure with the following parameters: TRIPOS force field without charge, 5 Å cutoff; 100 Simplex and 100 Powell iterations of SYBYL. All structural calculation and visualization were done on Silicon Graphics O2 or

Fuel graphical workstations. Coordinates of the models are available upon request from the authors.

RESULTS AND DISCUSSION

Several structural studies on separate domains of ErbB1-4 receptors were published recently, but it is still not known in molecular detail how ligand binding to the ErbB receptors leads to signal transduction. In this report we propose a model for a nearly full-length ErbB2 dimer, built by using FRET measurements, crystal structures of ErbB ectodomains, and molecular modeling methods. This model may supplement recent structural views (Burgess et al., 2003) to elucidate the molecular events of the ErbB signal transduction pathways.

Estimation of intermolecular epitope distances of ErbB2 molecules on N87 cells by FRET measurements

Homoassociation of ErbB2 molecules was determined by FRET measurements where Cy3- and Cy5-conjugated Herceptin Fab′ fragments were applied as a donor-acceptor pair. In the Fab′ molecules, the localization of the fluorophore was predetermined by an SH group introduced at the end distal from the antigen recognition site of the Fab′. The antibody fragments carried one fluorophore per molecule on average with a high degree of motional freedom allowing a dynamic orientational averaging. This condition allows a reasonable distance estimation from FRET efficiencies, since the statistical average of the orientation factor (otherwise also influencing FRET efficiency), $\kappa^2 = 2/3$, is a good approximation for this case. The FRET efficiency histograms constructed from cell-by-cell flow cytometric measurements (Fig. 1) show positive FRET efficiency for ErbB2 homoassociation on both cell lines (N87 and SK-BR-3), which differs significantly from the negative control, i.e., from the FRET efficiency distribution of the sample labeled with donor only. FRET analysis provided similar data for N87 and SK-BR-3 cells, but the expression level of ErbB2 was higher (30% more) on N87 than on SK-BR-3, thus only the data obtained on N87 cells are shown and used in this article. The FRET efficiency value ($11.2 \pm 0.9\%$ being the mean $\pm$ SD of histogram means from three independent measurements) was converted to molecular distances, as described in Materials and Methods. The intermolecular distance of Herceptin Fab′ on ErbB2 is 7.1 ± 0.2 nm, reflecting a close association of ErbB2 molecules on living N87 gastric carcinoma cells. Similar results were reported previously (Nagy et al., 1998, 2002), where whole IgGs were applied.

The distance of anti-ErbB2 Herceptin Fab′ from the plasma membrane

To determine the proximity of the ErbB2 ectodomain to the cell membrane, FRET experiments were performed with Alexa-488-labeled Herceptin Fab′ (with known docking site to the receptor) as a donor, and a lipid probe BODIPY-PC (581/591) as an acceptor with varying concentration and surface density. In addition, to verify our method for establishing proximities to the cell membrane, we also used a lipid probe (Cy5-DSPE) as a negative control, which only minimally enters the GM1-rich microdomains where ErbB2 is mostly localized, and obtained no considerable energy transfer efficiency values (2% with the highest concentration). The mean values of FRET efficiency distribution histograms were plotted as a function of lipid probe density and vertical distance from the membrane was derived from the slope of the fitted line, according to Yguerabide (1994) (Fig. 2). The fluorescently-labeled end part of Herceptin Fab′ had a closest approach distance of 7.5 ± 0.6 nm as a mean $\pm$ SD of three independent measurements. In the consequent molecular modeling, this distance estimate, measured on living cells, was used for steric positioning of the x-ray-resolved ErbB2 structures relative to the surface of the plasma membrane. Since we used a relative approach to determine the membrane proximity, the accuracy of the results might be in question. One source of uncertainty in the measurement of distance from the membrane is the calculation of surface concentration of the lipid probe. This calculation assumes perfectly spherical cells, although in reality the membrane is not even. Therefore the calculated surface concentration can be considered as the upper limit, and the true concentration of probe in the membrane should be more or less smaller, depending on the type of cells used in the experiments. The cells utilized in our experiments have a fairly smooth surface and, based on the good agreement of distances determined by two independent methods, the perfect sphere approximation appears to be a valid approach in this case. However, in the case of cells having substantially more uneven surfaces (e.g., macrophages), the distance obtained from the FRET measurement would be more overestimated and should be considered only as an upper limit of the distance. Since the region of the ErbB2 connecting the ectodomain with the transmembrane domain is quite flexible, the distance value measured for membrane proximity has little influence on our model calculations.

Construction of the model of ectodomain dimer of ErbB2

Chemical crosslinking experiments showed that ErbB1 formed a dimeric structure on the surface of living cells to some extent, without a bound ligand (Chu et al., 1997; Moriki et al., 2001). Partially purified ErbB1 was resolved in a sucrose density-gradient as mostly dimers in the presence of a low concentration of detergent (Moriki et al., 2001). Artificially mutated ErbB1 receptors containing Cys in the extracellular juxtamembrane region also showed a high tendency for dimerization (Moriki et al., 2001; Sorokin et al.,

1994). In situ FRET measurements on A431 epidermoid carcinoma cells confirmed the existence of preformed ErbB1 dimers in the cell membrane (Gadella and Jovin, 1995). Based on similar experiments on other ErbB molecules (Burke and Stern, 1998, Nagy et al., 1998, 2002), Moriki et al. (2001) assumed that the tendency for dimerization is valid not only for ErbB1, but also for other homologous members of ErbB family.

Our model-building procedure for ErbB2 dimer started with the extracellular domains of ErbB2. It was assumed that the ErbB2 dimer could adopt a conformation similar to that of the ErbB1 dimer in the crystal form (Ogiso et al., 2002). The fact that all kinds of homo- and heterodimerization can be seen among the members of the ErbB family (Yarden, 2001) and the similarities of the sequences and the structures of the dimerization arms of ErbB1–4 molecules, support this hypothesis. However, no such dimer formed during crystallization of the ErbB2 ectodomain (Cho et al., 2003; Garrett et al., 2003), which may suggest that interaction between ectodomains of ErbB2 is rather weak (Burgess et al., 2003). Also, although no homodimerization of the extracellular domains of ErbB2 was detected by sedimentation equilibrium analytical ultracentrifugation and multi-angle laser-light scattering, there was evidence for a weak ligand-induced heterodimerization with the extracellular domain of ErbB3 and ErbB4 (Ferguson et al., 2000). It was suggested by Garrett et al. (2003) that the ErbB2 ectodomain could not form a dimer similar to ErbB1 on its own, but multiple interactions could contribute to receptor association on the surface of living cells. However, flow cytometric resonance energy transfer measurements on living N87 cells showed some degree of ErbB2-ErbB2 ectodomain homoassociation: reproducible signals were measured between two differently labeled Herceptin Fab's, which can bind only to identical epitopes in the S2 domain of two ErbB2 ectodomains (Cho et al., 2003). Crystallographic analysis suggests that inhibition of signal transduction caused by Herceptin is not originated from a large structural change of ErbB2 ectodomain: uncomplexed human ErbB2 (Garrett et al., 2003) and rat ErbB2 (Cho et al., 2003) fragments form structures very similar to the Herceptin-complexed human ErbB2 (Cho et al., 2003) ectodomain.

There are four nonvisible loops in the crystal structure of ErbB2 ectodomain complexed with Herceptin Fab′ (Cho et al., 2003). Two of them (Ala^{302}–Thr^{306} and Asp^{360}–Ser^{365}) were modeled based on the homologous regions of the ErbB1 ectodomain (Ogiso et al., 2002). Another two loops (Leu^{101}–Ser^{111} and Ser^{580}–Ile^{591}) were built by the *Protein Loop Search* algorithm of SYBYL. Two copies of this ErbB2 model complexed with Herceptin Fab′ were aligned to the crystal structure of the ErbB1 dimer (Ogiso et al., 2002) A- and B-chains, respectively, and the conformations of the dimerization loops (Cys^{246}–Arg^{266}) were changed to those found in the ErbB1 dimer by MODELLER (Sali and Blundell, 1993). The alignment regions consisted of residues only from S1 domains (dimerization loops were also excluded), since different relative position of *L*- and *S*-domains in ErbB1 and ErbB2 may result in bad fitting of the two monomers (Fig. 3). Small bumps remained between the Herceptin Fab′ bound to the S2 domain of one monomer and the L2 domain of the other monomer, therefore ψ-torsional angles of Gly^{484} and Glu^{485} were changed from 331.5° to 335° and from 353.5° to 350°, respectively, in the flexible linker region between the L2 and S2 domains. To eliminate some large unfavorable van der Waals interactions generated by modeling, a short minimization was applied to the whole dimer. The dimer was translated and rotated to the center of the coordinate system in such a way that the C_2 symmetry axis of the dimer was in line with the *z* axis and the *x*,*y* plane served as a model for the outer surface of the cell membrane.

Although this dimer configuration appears to be a good candidate based on the analogy to the ErbB1 homodimer, it should be noted that other configurations for the ErbB2 homodimer should also exist so that the experimentally measured 7.1 nm intermolecular distance between bound Herceptin Fab′, which is substantially smaller than the 12.3 nm implied in the model, can also be satisfied. This 7.1 nm distance can be conceived as a weighted average from dimers predicted by the model and other dimers (or higher oligomers) that, themselves, would yield smaller intermolecular distances. Therefore it is predicted that the modeled

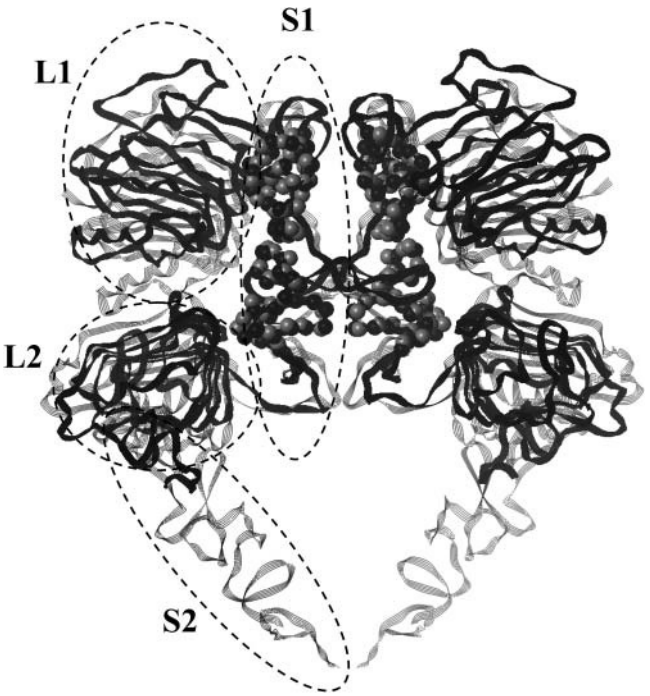

FIGURE 3 Ribbon models of superimposed ErbB1 (*solid ribbon*) and ErbB2 (*shaded ribbon*) ectodomains. Cα atoms that served as seed atoms for superposition are shown in space-fill representation in both structures. Domain names (*L1*, *S1*, *L2*, and *S2*) and approximate domain positions (*broken lines*) are shown only in one monomer.

ErbB1-like dimer configuration exists as a subclass among many others, and/or as a dynamic entity that could be interconverted to other dimeric forms. Sequence and structural differences between ErbB molecules may result in different levels of stabilization of various dimer forms that could exist at the same time.

Construction of the model for the transmembrane helix dimer of ErbB2

Besides the possible dimerization of ErbB2 ectodomains, the transmembrane domain can also dimerize, as supported by experimental data (Mendrola et al., 2002; Sharpe et al., 2002). Transmembrane α-helix pairs from membrane proteins with resolved structures served as a template for constructing the dimer of ErbB2 transmembrane domain. Two copies of the NMR structure of the transmembrane helix of ErbB2 (Goetz et al., 2001) were aligned to each helix-pair template and a short minimization was applied for each dimer of helices. The helix dimer which was based on helices 3 and 5 of the photosynthetic reaction center showed better agreement with requirements of the *GxxxG* dimerization motif and the models described previously (Fleishman et al., 2002; Gerber et al., 2004; Kim et al., 2003; Mendrola et al., 2002; Moriki et al., 2001); therefore it was chosen for further manipulation (Fig. 4).

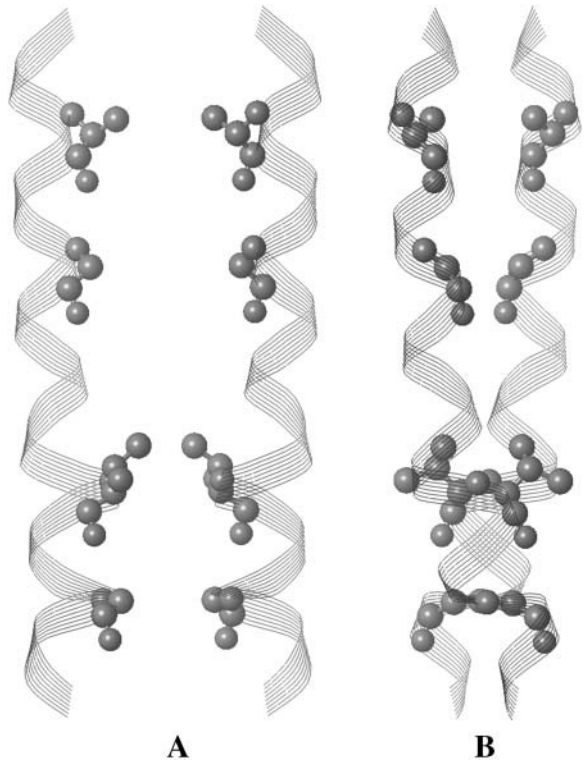

FIGURE 4 Front view (*A*) and side view (*B*) of the line ribbon model of transmembrane helix dimer. The outermost residues of the *GxxxG* motifs are shown in ball-and-stick representation in both monomers.

The helix dimer was positioned below the ectodomain dimer. The ectodomain dimer and the transmembrane dimer were put in the same rotational axis, therefore each dimer interface could enhance the effect of the other dimerization region. More than one dimerization interface, acting synergistically, may help the formation of tightly bound ErbB2 dimers or heterodimers with other members of the ErbB family and may help to find the correct position of kinase domains for transphosphorylation.

Construction of the model for the extracellular dimer of ErbB2

The distance between the ectodomain and the membrane was set based on FRET measurements: the ectodomain dimer complexed with Herceptin Fab′ was moved up along the *z* axis until the vertical distance of the free end of the Herceptin Fab′ from the cell membrane (*x*,*y* plane) reached the experimental value determined by FRET. The transmembrane helix dimer was moved down along the *z* axis until the N-terminal hydrophobic segment of the helices reached the *x*,*y* plane. The *Protein Loop Search* algorithm of SYBYL was applied to fill the gap between the C-terminal end of the ectodomain and the N-terminal end of the transmembrane domain. To satisfy the symmetry requirements of the structure, one monomer containing the full extracellular and transmembrane domains was duplicated and aligned to the other monomer, which was deleted after the transformation (Fig. 5). Short minimization was applied for the new dimer.

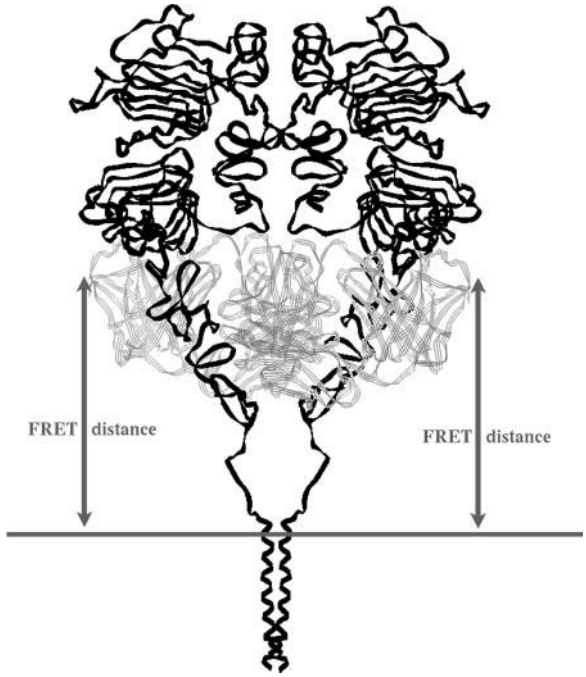

FIGURE 5 Ribbon model of the extracellular and transmembrane domains of ErbB2 (*solid ribbon*) complexed with Herceptin Fab′ (*shaded ribbon*). Arrows represent the distance of the end-labeled Herceptin Fab′ from the outer surface of the membrane (*horizontal line*) determined by FRET.

The C-terminal part of the S2 domain is not ordered, or does not exist in crystal structures of ErbB molecules (Cho and Leahy, 2002; Cho et al., 2003; Ferguson et al., 2003; Garrett et al., 2003, 2002; Ogiso et al., 2002), and may form a flexible arm together with the outer juxtamembrane region, as shown for the juxtamembrane region of ErbB1 (Moriki et al., 2001). The flexibility of this region may be required in dimer formation for the correct positioning of the first monomer (ErbB2) relative to the variable second monomer (ErbB1–4). Our flexible model does not rule out the possibility of interaction between S2 domains of homo- or heterodimers of ErbB molecules, as suggested by immunoprecipitation (Kumagai et al., 2003) and mutational studies (Siegel and Muller, 1996), and this possibility may also be valid for the linker regions.

Construction of the model for the intracellular dimer of ErbB2

Secondary structure of the juxtamembrane region located between the transmembrane and the protein kinase domains was predicted by several methods of SYBYL or of the ExPASy molecular biology server (http://www.expasy.org). All prediction methods showed high probability of α-helix for the N-terminal half of the sequence (Fig. 6).

Sequence similarity search against the Protein Data Bank was applied using the BLAST program of the ExPASy server. The top two hits were 1ETE and 3HLA. Both of them showed an elbowlike structure with an α-helical region on one side and an extended conformation on the other side. However, the α-helical region of the 1ETE fragment was located on the C-terminal, whereas the α-helical region of 3HLA fragment was located on the N-terminal part of the structure. The proximity of the α-helical transmembrane segment together with the consensus result of several secondary structure prediction methods and the three-dimensional structure of the 3HLA fragment suggested that this 3HLA fragment may serve as a good template for homologous modeling of the inner juxtamembrane region of ErbB2. The homologous model (Fig. 7) was built by MODELLER.

The inner juxtamembrane region seemed to be more rigid than the outer juxtamembrane region, which may help to transfer the molecular movement of the transmembrane domain toward the kinase domain. Rotational coupling of the transmembrane domain and kinase domains was shown experimentally for ErbB1 (Moriki et al., 2001) and ErbB2 (Bell et al., 2000).

```
                          TM  |        juxtamembrane          |  kinase
ErbB2 (648-691)           VFGILIKRRQQKIRKYTMRRLLQETELVEPLTPSGAMPNQAQMR
GOR                       ABBAAAAAAA---B-BBBBBAAAAAAABA----------AAAAB
Maxfield_Scheraga         ------AAAAAAAAAAAAAAAA-AAAA----------------
Qian_Sejnowski            ---BBAAAA-AAAAAAAAAAAA----------------------
GOR4                      ---BBB-AAAAAAAAAAAAAAAAAAA--------------BBB-
Jnet                      -------AAAAAAAAAAAAAAAAAAAA----------------
SOPMA                     BBBBBBA---AAAAAAAAAAAAAAAAAA------------AAAA
HNN                       --BBBAAAAAAAAAAAAAAAAAAAAA----------------
X-ray                     AAAAAAAAAA----------------------BBBBBBBBBB
```

FIGURE 6 Secondary structure prediction of inner juxtamembrane region of ErbB2 using different methods. Only α-helical (A) and β-sheet (B) states are shown.

FIGURE 7 Homologous model of the inner juxtamembrane region of ErbB2.

Two copies of the model of the juxtamembrane segment were superimposed with the modeled transmembrane helix dimer using the four N-terminal residues, which were common in the models of the juxtamembrane region and the transmembrane helix. Model building was continued with the superposition of two copies of the protein kinase domain using the common four terminal residues. Interestingly, using this approach, the two kinase domains formed a good, symmetric back-to-back dimer without any unfavorable interaction (Fig. 8, *A* and *B*). A short minimization procedure was applied for the whole intracellular dimer as previously done for the extracellular dimer.

In our model the localization of the kinase domain was designated solely based on the position of the transmembrane domain dimer and the shape of the model of the inner juxtamembrane region. Based on the model, kinase domains may interact and may serve as a third dimerization interface.

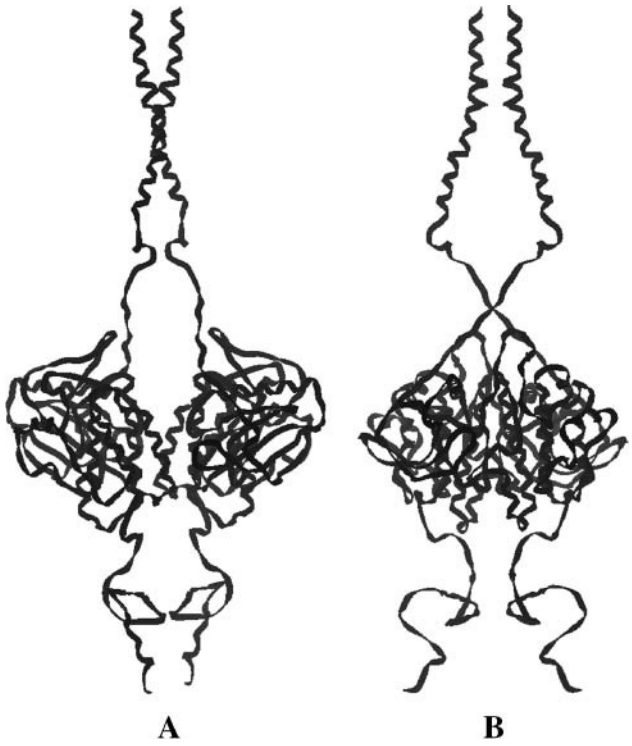

FIGURE 8 Front view (*A*) and side view (*B*) of the ribbon model of the transmembrane and the intracellular domains of the assumed ErbB2 dimer.

The interaction of kinase domains is also supported by experimental data (Penuel et al., 2002).

We searched PDB for similar configurations of protein kinase dimers, but there were none in which the two monomers occupied the same relative position as in our model. We also checked the other four transmembrane helix dimers which were neglected previously. If the transmembrane region and the kinase domain were linked with the same elbowlike structure, they resulted in too close or too distant kinase domains, which were unable to interact with each other in the dimer configuration.

Construction of the nearly full-length model for the ErbB2 dimer

The models of the extracellular dimer and intracellular dimer were superimposed based on the common transmembrane regions. This nearly full-length ErbB2 dimer consisted of the whole ectodomain, the outer juxtamembrane region, the transmembrane domain, the inner juxtamembrane region, the protein kinase domain, and a part of the regulatory C-terminal tail of the ErbB2 molecule (Fig. 9).

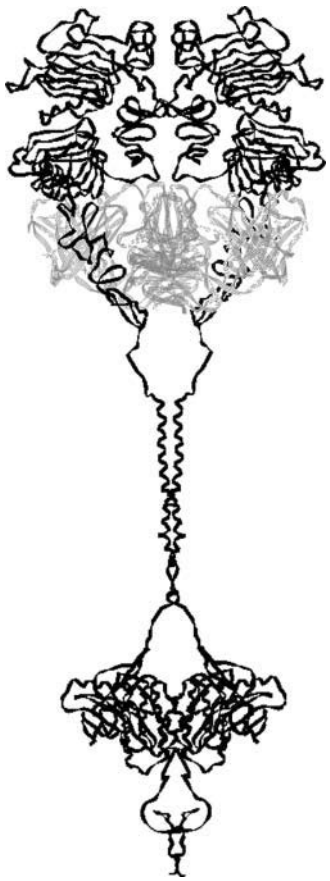

FIGURE 9 Ribbon representation of the model of the nearly full-length ErbB2 homodimer (*solid ribbon*) complexed with Herceptin Fab′ (*shaded ribbon*).

We have built an ErbB2 homodimer structure with three potentially interacting regions. This ErbB2 homodimer, taking into account the similar structures of the ligand-bound forms of the other ErbB molecules, may serve as a starting model for heterodimers of ErbB2 with other members of the ErbB family. It should be noted that even higher levels of associations might be required for signal transduction through the ErbB receptors. The back-to-back kinase dimer arrangement could be responsible for the transphosphorylation of the cytoplasmic regulatory tails but not of the kinase domains themselves, which requires the involvement of other kinase molecules.

CONCLUSION

Here we report a procedure that combines existing crystal structures, NMR data, and FRET measurements with molecular modeling to predict an almost full-length monomeric, as well as possible dimeric forms for ErbB2 (and other ErbB) receptors. It should be emphasized that our predicted ErbB dimer structure could be just one of the several possibilities that may exist on the surface of a living cell: other types of dimer configurations should exist which satisfy the FRET distance criteria alone, or in combination. The resolution of our model is not aimed to reach the resolution of the initial crystal structures, especially not in the linker regions and at the dimer interfaces, but it may serve as a working hypothesis and may initiate experiments to confirm or reject it. A crucial part of our modeling was the incorporation of FRET data obtained on live cells into the construction of the nearly full-length ErbB2 model.

We thank Prof. A.W. Burgess (Ludwig Institute for Cancer Research, Royal Melbourne Hospital, Victoria, Australia) for providing the three-dimensional coordinates of ErbB1 structure before their publication.

This work was supported by grants of the Fifth Framework Program of the European Union (EU FP5 QLGI-CT-2000-1260), the Hungarian Medical Research Council (ETT (524/2003, 532/2003), and the Hungarian Scientific Research Fund (OTKA (T037831, T043061, T043482).

REFERENCES

Bastiaens, P. I., and T. M. Jovin. 1996. Microspectroscopic imaging tracks the intracellular processing of a signal transduction protein: fluorescent-labeled protein kinase C beta I. *Proc. Natl. Acad. Sci. USA.* 93: 8407–8412.

Bell, C. A., J. A. Tynan, K. C. Hart, A. N. Meyer, S. C. Robertson, and D. J. Donoghue. 2000. Rotational coupling of the transmembrane and kinase domains of the Neu receptor tyrosine kinase. *Mol. Biol. Cell.* 11: 3589–3599.

Berman, H. M., J. Westbrook, Z. Feng, G. Gilliland, T. N. Bhat, H. Weissig, I. N. Shindyalov, and P. E. Bourne. 2000. The Protein Data Bank. *Nucleic Acids Res.* 28:235–242.

Blume-Jensen, P., and T. Hunter. 2001. Oncogenic kinase signalling. *Nature.* 411:355–365.

Burgess, A. W., H. S. Cho, C. Eigenbrot, K. M. Ferguson, T. P. Garrett, D. J. Leahy, M. A. Lemmon, M. X. Sliwkowski, C. W. Ward, and S.

Yokoyama. 2003. An open-and-shut case? Recent insights into the activation of EGF/ErbB receptors. *Mol. Cell.* 12:541–552.

Burke, C. L., and D. F. Stern. 1998. Activation of Neu (ErbB-2) mediated by disulfide bond-induced dimerization reveals a receptor tyrosine kinase dimer interface. *Mol. Cell. Biol.* 18:5371–5379.

Carter, P., B. M. Fendly, G. D. Lewis, and M. X. Sliwkowski. 1999. Development of Herceptin. *Breast Disease.* 11:103–111.

Carter, P., L. Presta, C. M. Gorman, J. B. Ridgway, D. Henner, W. L. Wong, A. M. Rowland, C. Kotts, M. E. Carver, and H. M. Shepard. 1992. Humanization of an anti-p185HER2 antibody for human cancer therapy. *Proc. Natl. Acad. Sci. USA.* 89:4285–4289.

Cho, H. S., and D. J. Leahy. 2002. Structure of the extracellular region of HER3 reveals an interdomain tether. *Science.* 297:1330–1333.

Cho, H. S., K. Mason, K. X. Ramyar, A. M. Stanley, S. B. Gabelli, D. W. Denney, Jr., and D. J. Leahy. 2003. Structure of the extracellular region of HER2 alone and in complex with the Herceptin Fab. *Nature.* 421: 756–760.

Chu, C. T., K. D. Everiss, C. J. Wikstrand, S. K. Batra, H. J. Kung, and D. D. Bigner. 1997. Receptor dimerization is not a factor in the signalling activity of a transforming variant epidermal growth factor receptor (EGFRvIII). *Biochem. J.* 324:855–861.

Citri, A., K. B. Skaria, and Y. Yarden. 2003. The deaf and the dumb: the biology of ErbB-2 and ErbB-3. *Exp. Cell Res.* 284:54–65.

Cuff, J. A., and G. J. Barton. 1999. Evaluation and improvement of multiple sequence methods for protein secondary structure prediction. *Proteins.* 34:508–519.

de Bono, J. S., and E. K. Rowinsky. 2002. The ErbB receptor family: a therapeutic target for cancer. *Trends Mol. Med.* 8(4 Suppl):S19–S26.

Deisenhofer, J., O. Epp, I. Sinning, and H. Michel. 1995. Crystallographic refinement at 2.3 Å resolution and refined model of the photosynthetic reaction centre from *Rhodopseudomonas viridis*. *J. Mol. Biol.* 246: 429–457.

Ferguson, K. M., M. B. Berger, J. M. Mendrola, H. S. Cho, D. J. Leahy, and M. A. Lemmon. 2003. EGF activates its receptor by removing interactions that autoinhibit ectodomain dimerization. *Mol. Cell.* 11: 507–517.

Ferguson, K. M., P. J. Darling, M. J. Mohan, T. L. Macatee, and M. A. Lemmon. 2000. Extracellular domains drive homo- but not hetero-dimerization of ErbB receptors. *EMBO J.* 19:4632–4643.

Fleishman, S. J., J. Schlessinger, and N. Ben-Tal. 2002. A putative molecular-activation switch in the transmembrane domain of ErbB2. *Proc. Natl. Acad. Sci. USA.* 99:15937–15940.

Förster, T. 1948. Intermolecular energy transfer and fluorescence. *Annal. Physik.* 2:55–75.

Förster, T. 1949. Experimental and theoretical investigation of intermolecular transfer of electronic excitiation energy. *Z. Naturforsch.* 4a:321–327.

Gadella, T. W., Jr., and T. M. Jovin. 1995. Oligomerization of epidermal growth factor receptors on A431 cells studied by time-resolved fluorescence imaging microscopy. A stereochemical model for tyrosine kinase receptor activation. *J. Cell Biol.* 129:1543–1558.

Garnier, J., J. F. Gibrat, and B. Robson. 1996. GOR method for predicting protein secondary structure from amino acid sequence. *Methods Enzymol.* 266:540–553.

Garnier, J., D. J. Osguthorpe, and B. Robson. 1978. Analysis of the accuracy and implications of simple methods for predicting the secondary structure of globular proteins. *J. Mol. Biol.* 120:97–120.

Garrett, T. P., N. M. McKern, M. Lou, T. C. Elleman, T. E. Adams, G. O. Lovrecz, M. Kofler, R. N. Jorissen, E. C. Nice, A. W. Burgess, and C. W. Ward. 2003. The crystal structure of a truncated ErbB2 ectodomain reveals an active conformation, poised to interact with other ErbB receptors. *Mol. Cell.* 11:495–505.

Garrett, T. P., N. M. McKern, M. Lou, T. C. Elleman, T. E. Adams, G. O. Lovrecz, H. J. Zhu, F. Walker, M. J. Frenkel, P. A. Hoyne, and R. N. Jorissen, E. C. Nice, A. W. Burgess, and C. W. Ward. 2002. Crystal structure of a truncated epidermal growth factor receptor extracellular domain bound to transforming growth factor alpha. *Cell.* 110:763–773.

Gáspár, R., Jr., P. Bagossi, L. Bene, J. Matkó, J. Szöllösi, J. Tözsér, L. Fésüs, T. A. Waldmann, and S. Damjanovich. 2001. Clustering of class I HLA oligomers with CD8 and TCR: three-dimensional models based on fluorescence resonance energy transfer and crystallographic data. *J. Immunol.* 166:5078–5086.

Geourjon, C., and G. Deleage. 1995. SOPMA: significant improvements in protein secondary structure prediction by consensus prediction from multiple alignments. *Comput. Appl. Biosci.* 11:681–684.

Gerber, D., N. Sal-Man, and Y. Shai. 2004. Two motifs within a transmembrane domain—one for homodimerization and the other for heterodimerization. *J. Biol. Chem.* 279:21177–21182.

Goetz, M., C. Carlotti, F. Bontems, and E. J. Dufourc. 2001. Evidence for an α-helix $\rightarrow$ π-bulge helicity modulation for the Neu/ErbB-2 membrane-spanning segment. A 1H-NMR and circular dichroism study. *Biochemistry.* 40:6534–6540.

Guermeur, Y., C. Geourjon, P. Gallinari, and G. Deleage. 1999. Improved performance in protein secondary structure prediction by inhomogeneous score combination. *Bioinformatics.* 15:413–421.

Jackson, J. G., P. St Clair, M. X. Sliwkowski, and M. G. Brattain. 2004. Blockade of epidermal growth factor- or heregulin-dependent ErbB2 activation with the anti-ErbB2 monoclonal antibody 2C4 has divergent downstream signaling and growth effects. *Cancer Res.* 64:2601–2609.

Kim, S., A. K. Chamberlain, and J. U. Bowie. 2003. A simple method for modeling transmembrane helix oligomers. *J. Mol. Biol.* 329:831–840.

Koeppen, H. K., B. D. Wright, A. D. Burt, P. Quirke, A. M. McNicol, N. O. Dybdal, M. X. Sliwkowski, and K. J. Hillan. 2001. Overexpression of HER2/Neu in solid tumours: an immunohistochemical survey. *Histopathology.* 38:96–104.

Kumagai, T., M. Katsumata, A. Hasegawa, K. Furuuchi, T. Funakoshi, I. Kawase, and M. I. Greene. 2003. Role of extracellular subdomains of p185c-Neu and the epidermal growth factor receptor in ligand-independent association and transactivation. *Proc. Natl. Acad. Sci. USA.* 100:9220–9225.

Kute, T., C. M. Lack, M. Willingham, B. Bishwokama, H. Williams, K. Barrett, T. Mitchell, and J. P. Vaughn. 2004. Development of Herceptin resistance in breast cancer cells. *Cytometry.* 57A:86–93.

MacKenzie, K. R., J. H. Prestegard, and D. M. Engelman. 1997. A transmembrane helix dimer: structure and implications. *Science.* 276: 131–133.

Marmor, M. D., K. B. Skaria, and Y. Yarden. 2004. Signal transduction and oncogenesis by ErbB/HER receptors. *Int. J. Radiat. Oncol. Biol. Phys.* 58:903–913.

Maxfield, F. R., and H. A. Scheraga. 1976. Status of empirical methods for the prediction of protein backbone topography. *Biochemistry.* 15: 5138–5153.

Mendrola, J. M., M. B. Berger, M. C. King, and M. A. Lemmon. 2002. The single transmembrane domains of ErbB receptors self-associate in cell membranes. *J. Biol. Chem.* 277:4704–4712.

Moriki, T., H. Maruyama, and I. N. Maruyama. 2001. Activation of preformed EGF receptor dimers by ligand-induced rotation of the transmembrane domain. *J. Mol. Biol.* 311:1011–1026.

Nagy, P., L. Bene, M. Balázs, W. C. Hyun, S. J. Lockett, N. Y. Chiang, F. Waldman, B. G. Feuerstein, S. Damjanovich, and J. Szöllösi. 1998. EGF-induced redistribution of ErbB2 on breast tumor cells: flow and image cytometric energy transfer measurements. *Cytometry.* 32:120–131.

Nagy, P., G. Vereb, Z. Sebestyén, G. Horváth, S. J. Lockett, S. Damjanovich, J. W. Park, T. M. Jovin, and J. Szöllösi. 2002. Lipid rafts and the local density of ErbB proteins influence the biological role of homo- and heteroassociations of ErbB2. *J. Cell Sci.* 115:4251–4262.

Ogiso, H., R. Ishitani, O. Nureki, S. Fukai, M. Yamanaka, J. H. Kim, K. Saito, A. Sakamoto, M. Inoue, M. Shirouzu, and S. Yokoyama. 2002. Crystal structure of the complex of human epidermal growth factor and receptor extracellular domains. *Cell.* 110:775–787.

Paik, S., and E. T. Liu. 1999. HER2 as a predictor of therapeutic response in breast cancer. *Breast Disease.* 11:91–102.

Pebay-Peyroula, E., G. Rummel, J. P. Rosenbusch, and E. M. Landau. 1997. X-ray structure of bacteriorhodopsin at 2.5 Ångstroms from microcrystals grown in lipidic cubic phases. *Science*. 277:1676–1681.

Penuel, E., R. W. Akita, and M. X. Sliwkowski. 2002. Identification of a region within the ErbB2/HER2 intracellular domain that is necessary for ligand-independent association. *J. Biol. Chem.* 277:28468–28473.

Press, M. F., M. C. Pike, G. Hung, J. Y. Zhou, Y. Ma, J. George, J. Dietz-Band, W. James, D. J. Slamon, and J. G. Batsakis. 1994. Amplification and overexpression of HER-2/Neu in carcinomas of the salivary gland: correlation with poor prognosis. *Cancer Res.* 54:5675–5682.

Qian, N., and T. J. Sejnowski. 1988. Predicting the secondary structure of globular proteins using neural network models. *J. Mol. Biol.* 202: 865–884.

Ranson, M., and M. X. Sliwkowski. 2002. Perspectives on anti-HER monoclonal antibodies. *Oncology*. 63(Suppl 1):17–24.

Ross, J. S., and J. A. Fletcher. 1998. The HER-2/Neu oncogene in breast cancer: prognostic factor, predictive factor, and target for therapy. *Oncologist*. 3:237–252.

Sali, A., and T. L. Blundell. 1993. Comparative protein modelling by satisfaction of spatial restraints. *J. Mol. Biol.* 234:779–815.

Schlessinger, J. 2000. Cell signaling by receptor tyrosine kinases. *Cell*. 103:211–225.

Sebestyén, Z., P. Nagy, G. Horváth, G. Vámosi, R. Debets, J. W. Gratama, D. R. Alexander, and J. Szöllösi. 2002. Long wavelength fluorophores and cell-by-cell correction for autofluorescence significantly improves the accuracy of flow cytometric energy transfer measurements on a dual-laser benchtop flow cytometer. *Cytometry*. 48:124–135.

Sharpe, S., K. R. Barber, and C. W. Grant. 2002. Evidence of a tendency to self-association of the transmembrane domain of ErbB-2 in fluid phospholipid bilayers. *Biochemistry*. 41:2341–2352.

Siegel, P. M., and W. J. Muller. 1996. Mutations affecting conserved cysteine residues within the extracellular domain of Neu promote receptor dimerization and activation. *Proc. Natl. Acad. Sci. USA*. 93: 8878–8883.

Slamon, D. J., G. M. Clark, S. G. Wong, W. J. Levin, A. Ullrich, and W. L. McGuire. 1987. Human breast cancer: correlation of relapse and survival with amplification of the HER-2/Neu oncogene. *Science*. 235:177–182.

Slamon, D. J., W. Godolphin, L. A. Jones, J. A. Holt, S. G. Wong, D. E. Keith, W. J. Levin, S. G. Stuart, J. Udove, A. Ullrich, and M. F. Press. 1989. Studies of the HER-2/Neu proto-oncogene in human breast and ovarian cancer. *Science*. 244:707–712.

Sorokin, A., M. A. Lemmon, A. Ullrich, and J. Schlessinger. 1994. Stabilization of an active dimeric form of the epidermal growth factor receptor by introduction of an inter-receptor disulfide bond. *J. Biol. Chem.* 269:9752–9759.

Stamos, J., M. X. Sliwkowski, and C. Eigenbrot. 2002. Structure of the epidermal growth factor receptor kinase domain alone and in complex with a 4-anilinoquinazoline inhibitor. *J. Biol. Chem.* 277:46265–46272.

Szentesi, G., G. Horváth, I. Bori, G. Vámosi, J. Szöllösi, R. Gáspár, S. Damjanovich, A. Jenei, and L. Mátyus. 2004. Computer program for determining fluorescence resonance energy transfer efficiency from flow cytometric data on a cell-by-cell basis. *Comput. Methods Programs Biomed.* 75:201–211.

Szöllösi, J., V. Horejsi, L. Bene, P. Angelisova, and S. Damjanovich. 1996. Supramolecular complexes of MHC class I, MHC class II, CD20, and tetraspan molecules (CD53, CD81, and CD82) at the surface of a B cell line JY. *J. Immunol.* 157:2939–2946.

Szöllösi, J., P. Nagy, Z. Sebestyén, S. Damjanovich, J. W. Park, and L. Mátyus. 2002. Applications of fluorescence resonance energy transfer for mapping biological membranes. *J. Biotechnol.* 82:251–266.

Szöllösi, J., L. Trón, S. Damjanovich, S. H. Helliwell, D. Arndt-Jovin, and T. M. Jovin. 1984. Fluorescence energy transfer measurements on cell surfaces: a critical comparison of steady-state fluorimetric and flow cytometric methods. *Cytometry*. 5:210–216.

Thompson, J. D., D. G. Higgins, and T. J. Gibson. 1994. CLUSTAL W: improving the sensitivity of progressive multiple sequence alignment through sequence weighting, position-specific gap penalties and weight matrix choice. *Nucleic Acids Res.* 22:4673–4680.

Trón, L., J. Szöllösi, S. Damjanovich, S. H. Helliwell, D. J. Arndt-Jovin, and T. M. Jovin. 1984. Flow cytometric measurement of fluorescence resonance energy transfer on cell surfaces. Quantitative evaluation of the transfer efficiency on a cell-by-cell basis. *Biophys. J.* 45:939–946.

Valenzuela, C. F., P. Weign, J. Yguerabide, and D. A. Johnson. 1994. Transverse distance between the membrane and the agonist binding sites on the *Torpedo* acetylcholine receptor: a fluorescence study. *Biophys. J.* 66:674–682.

Vereb, G., P. Nagy, J. W. Park, and J. Szöllösi. 2002. Signaling revealed by mapping molecular interactions: implications for ErbB-targeted cancer immunotherapies. *Clin. Appl. Immunol. Rev.* 2:169–186.

Vereb, G., J. Szöllösi, J. Matkó, P. Nagy, T. Farkas, L. Vigh, L. Mátyus, T. A. Waldmann, and S. Damjanovich. 2003. Dynamic, yet structured: the cell membrane three decades after the Singer-Nicolson model. *Proc. Natl. Acad. Sci. USA*. 100:8053–8058.

Yarden, Y. 2001. The EGFR family and its ligands in human cancer. Signalling mechanisms and therapeutic opportunities. *Eur. J. Cancer*. 37:S3–S8.

Yguerabide, J. 1994. Theory for establishing proximity relations in biological membranes by excitation energy transfer measurements. *Biophys. J.* 66:683–693.